

The Fine Structure Lines of Hydrogen in HII Regions

Brian Dennison

*Physics Department, and Pisgah Astronomical Research and Science Education Center,
University of North Carolina at Asheville, Asheville, NC 28804*

dennison@unca.edu

B. E. Turner

National Radio Astronomy Observatory, 520 Edgement Road, Charlottesville, VA 22903-2475

bturner@nrao.edu

Anthony H. Minter

National Radio Astronomy Observatory, P. O. Box 2, Green Bank, WV 24944

tminter@nrao.edu

ABSTRACT

The $2s_{1/2}$ state of hydrogen is metastable and overpopulated in HII regions. In addition, the $2p$ states may be pumped by ambient Lyman- α radiation. Fine structure transitions between these states may be observable in HII regions at 1.1 GHz ($2s_{1/2} - 2p_{1/2}$) and/or 9.9 GHz ($2s_{1/2} - 2p_{3/2}$), although the details of absorption versus emission are determined by the relative populations of the $2s$ and $2p$ states. The $n = 2$ level populations are solved with a parameterization that allows for Lyman- α pumping of the $2p$ states. The Lyman- α pumping rate has long been considered uncertain as it involves solution of the difficult Lyman- α transfer problem. The density of Lyman- α photons is set by their creation rate, easily determined from the recombination rate, and their removal rate. Here we suggest that the dominant removal mechanism of Lyman- α radiation in HII regions is absorption by dust. This circumvents the need to solve the Lyman- α transfer problem, and provides an upper limit to the rate at which the $2p$ states are populated by Lyman- α photons. In virtually all cases of interest, the $2p$ states are predominantly populated by recombination, rather than Lyman- α pumping. We then solve the radiative transfer problem for the fine structure lines in the presence of free-free radiation. In the likely absence of Lyman- α pumping, the $2s_{1/2} \rightarrow 2p_{1/2}$ lines will appear in stimulated emission and the $2s_{1/2} \rightarrow 2p_{3/2}$ lines in absorption. Because the final $2p$ states are short lived these lines are dominated by intrinsic linewidth (99.8 MHz). In addition, each fine structure line is a multiplet of three blended hyperfine transitions. Searching for the 9.9 GHz lines in high emission

measure HII regions offers the best prospects for detection. The lines are predicted to be weak; in the best cases, line-to continuum ratios of several tenths of a percent might be expected with line strengths of tens to a hundred mK with the Green Bank Telescope. Predicted line strengths, at both 1.1 and 9.9 GHz, are given for a number of HII regions, high emission measure components, and planetary nebulae, based upon somewhat uncertain emission measures, sizes, and structures. The extraordinary width of these lines and their blended structure will complicate detection.

Subject headings: ISM: HII regions — ISM: lines and bands — line: formation — planetary nebulae: general — radio lines: ISM

1. Introduction

Transitions between fine-structure sublevels in atomic hydrogen have never been detected astronomically. With advances in radio astronomy, however, it now appears that transitions between the $2s_{1/2}$ and $2p_{1/2}$, and $2s_{1/2}$ and $2p_{3/2}$ levels may soon be observable in HII regions. Figure 1 shows the fine and hyperfine structure of the $n = 2$ level of atomic hydrogen. The fine structure splitting into the $2s_{1/2}$, $2p_{1/2}$, and $2p_{3/2}$ levels is caused by a combination of spin orbit coupling, relativistic effects and the Lamb shift. Significantly, the $2s_{1/2}$ state is metastable owing to the transition rules for angular momentum, i.e. the $2s-1s$ transition is forbidden. Hydrogen atoms in the interstellar medium are removed from the $2s_{1/2}$ state principally through 2-photon emission to the ground state (Breit and Teller 1940) with decay rate per atom, $A_{2\gamma} = 8.227\text{sec}^{-1}$ (Spitzer and Greenstein 1951), resulting in optical continuum radiation. Because this rate is some eight orders of magnitude slower than Lyman decay, it may seem reasonable to expect that the $2s_{1/2}$ state will be overpopulated relative to other excited states under photoionization equilibrium. It must be noted, however, that trapped Lyman- α radiation in an HII region will pump the $2p$ states. In addition, in dense HII regions collisions, primarily with ions, will transfer hydrogen atoms between the $2s$ and $2p$ states. These effects must be taken into account in order to determine the expected strengths and signs (absorption versus stimulated emission) of the $2s_{1/2}-2p_{1/2}$ (1.1 GHz) and $2s_{1/2}-2p_{3/2}$ (9.9 GHz) lines.

Apparently, Wild (1952) was one of the first to investigate the astrophysical implications of these lines, suggesting that the $2s_{1/2}-2p_{3/2}$ line might be observed in the sun. Purcell (1952), however, noted that collisions in the dense solar atmosphere would equilibrate the $2s$ and $2p$ populations making detection unlikely. Townes (1957) suggested that an overpopulation of the metastable $2s$ states may lead to detectable lines in the interstellar medium. Shklovsky (1960) raised the possibility of Lyman- α pumping of the $2p$ states but discounted its sufficiency for producing observable $2p \rightarrow 2s$ transitions. Pottasch (1960) argued that the Lyman- α depth in HII regions is essentially infinite such that virtually all downward Lyman- α transitions are balanced by a Lyman- α absorption, resulting in an overpopulation of $2p$ states relative to $2s$ at densities below about 10^4 cm^{-3} .

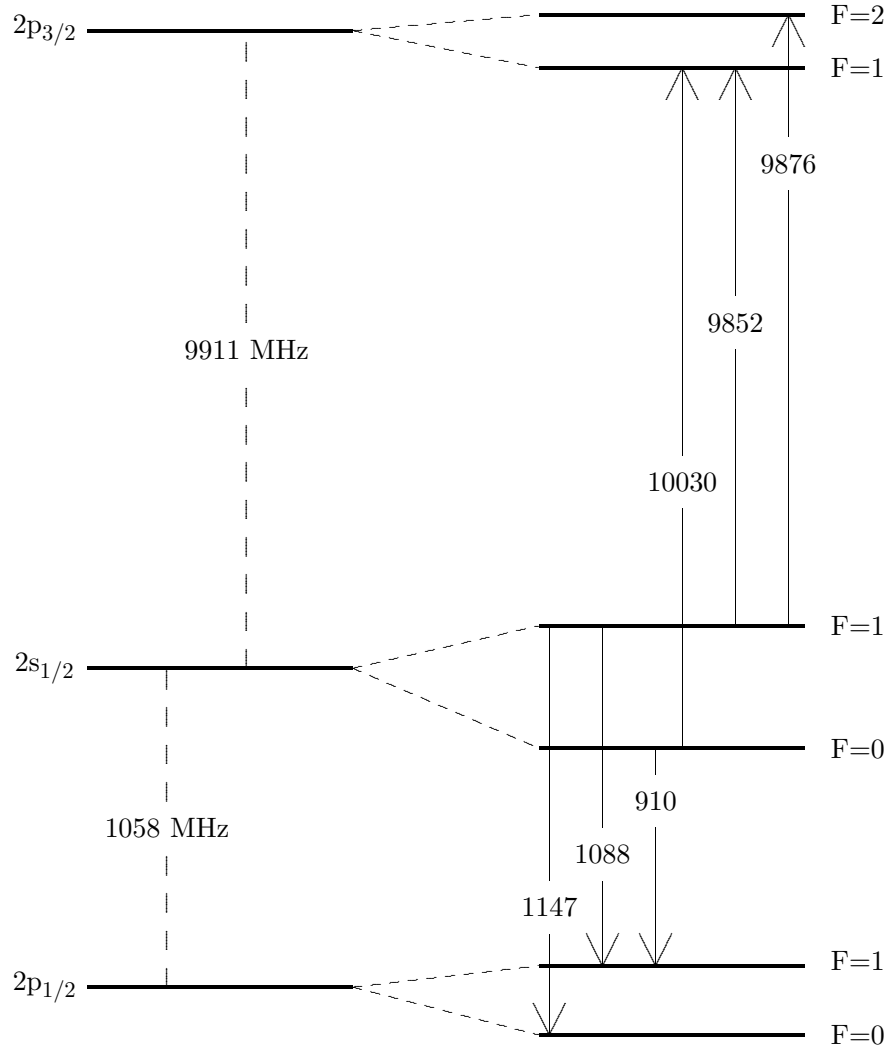


Fig. 1.— Fine and hyperfine structure of the $n = 2$ level of hydrogen. Allowed hyperfine transitions are shown as solid vertical lines, with arrows denoting predominant transition directions if the metastable $2s_{1/2}$ states are overpopulated with respect to the $2p$ states. (See text.) Hyperfine transition frequencies are given in MHz. The quantum number F corresponds to total angular momentum, i.e., orbit + electron spin + nuclear spin. Note that level separations are not shown to scale.

Field and Partridge (1961) further considered the case in which Lyman- α radiation is effectively destroyed by collisional conversion of $2p$ states to $2s$ (followed by 2-photon decay to the ground state). The consequent overpopulation of $2p$ states then led to the prediction that the 9.9 GHz lines would appear in stimulated emission in HII regions. (This also implied that the 1.1 GHz lines would appear in absorption.) Myers and Barrett (1972) used the Haystack 37-m radiotelescope with a 16-channel filter bank spanning 1 GHz in frequency to search for the 9.9 GHz lines, but did not find any lines in excess of 0.1 K antenna temperature.

The major uncertainty in the various predictions stems from the uncertain density of Lyman- α radiation in HII regions, which in turn is determined by the processes that destroy Lyman- α radiation. In addition to the conversion of $2p$ to $2s$ states via collisions, other processes are likely to be important. Resonantly scattered Lyman- α photons undergo a diffusion in frequency and may thus acquire a significant probability of escaping the HII region due the much lower optical depth in the line wings (Cox and Matthews 1969, Spitzer 1978). Systematic gas motions within the region (e.g. expansion) can also contribute to the migration of Lyman- α photons away from line center. The dominant removal mechanism, however, is absorption by dust within the HII region (Spitzer 1978). This last fact greatly simplifies the estimation of the Lyman- α density.

In this paper, we obtain formulae for the $2s$ and $2p$ populations in an HII region under a parameterization that characterizes the rate of $2p$ production by Lyman- α absorption in terms of the rate of $2p$ production through recombination (Section 2). Existing models for dust in HII regions and planetary nebulae are then used to place tight constraints on the Lyman- α density and thus the $2p$ production rate by Lyman- α photons (Section 3). The radiative transfer problem for the fine structure lines is then solved for a uniform region (Section 4). We obtain approximate predicted line strengths for various HII regions, compact components, and planetary nebulae under the justified assumption that Lyman- α pumping of the $2p$ states is negligible (Section 5). High emission measure HII regions and/or planetary nebulae are most likely to yield detectable lines.

2. Population of the $2s$ and $2p$ States

Spitzer & Greenstein (1951) estimated that between 0.30 and 0.35 of all recombinations in an HII region reach the $2s$ state. Including the effects of collisions and the 2-photon decay rate, the rate equation for the $2s$ state is

$$f\alpha n_i n_e + C_{ps} n_i n_{2p} = A_{2\gamma} n_{2s} + C_{sp} n_i n_{2s}, \quad (1)$$

where f is the fraction of recombinations producing the $2s$ state and α is the recombination coefficient. The collision coefficients, C_{ps} and C_{sp} , give the appropriate rates at which atoms are transferred from $2p$ to $2s$ and from $2s$ to $2p$, respectively. These rates are dominated by collisions with protons, but including electron collisions (and assuming that $n_e = n_i$ and $T = 10^4$ K), we have $C_{sp} = 5.31 \times 10^{-4} \text{ cm}^3 \text{ s}^{-1}$ (Seaton 1955). Since kT is much greater than the energy separations between the $2s$ and $2p$ states, the reverse rate is determined by just the ratio of statistical weights,

i.e.

$$C_{ps} = \frac{g_{2s}}{g_{2p}} C_{sp} = \frac{1}{3} C_{sp}. \quad (2)$$

Similar considerations apply to the $2p$ states. The fraction of recombinations reaching $2p$ is $(1 - f)$. [It is worth noting that processes such as Lyman- β absorption, which ultimately produce the $2s$ state through $1s \rightarrow 3p \rightarrow 2s$, have already been taken into account in the calculation of f (Spitzer & Greenstein 1951).] Radiative decay occurs through both spontaneous Lyman- α emission (with $A_{21} = 6.25 \times 10^8 \text{ sec}^{-1}$), as well as stimulated emission. We must also include radiative excitation from the ground state via Lyman- α absorption. Including collisions which couple to the $2s$ states, the rate equation for $2p$ then is

$$\begin{aligned} (1 - f)\alpha n_i n_e + C_{sp} n_i n_{2s} + c \int n_\nu^{(1s)} d\nu \int B_{12}(\nu - \nu') n_{\nu'} d\nu' \\ = A_{21} n_{2p} + C_{ps} n_i n_{2p} + c \int n_\nu^{(2p)} d\nu \int B_{21}(\nu - \nu') n_{\nu'} d\nu', \end{aligned} \quad (3)$$

where $n_\nu^{(1s)}$ and $n_\nu^{(2p)}$ are the densities of atoms in the $1s$ and $2p$ states per radial velocity interval, measured in frequency units; and $n_{\nu'}$ is the photon density per frequency interval (in $\text{cm}^{-3} \text{ Hz}^{-1}$). Now,

$$B_{21}(\nu - \nu') = \frac{c^2}{8\pi\nu_L^2} A_{21} L(\nu - \nu') \quad (4)$$

$$\text{and } B_{12}(\nu - \nu') = 3B_{21}(\nu - \nu'), \quad (5)$$

where ν_L is the Lyman- α frequency, and $L(\nu - \nu')$ is the Lorentz line profile. For a thermal gas,

$$n_\nu^{(1s)} = \frac{n_{1s}}{\sqrt{\pi}(\Delta\nu)_D} e^{-\frac{(\nu-\nu_0)^2}{(\Delta\nu)_D^2}}, \quad (6)$$

where $(\Delta\nu)_D$ is the Doppler width. For $T = 10^4 \text{ K}$, $(\Delta\nu)_D = 1.29 \times 10^{11} \text{ Hz}$. Clearly thermal widths will completely dominate the natural (Lorentz) line width of Lyman- α , and thus we can replace $L(\nu - \nu')$ by the Dirac delta function. We then obtain for the absorption term:

$$c \int n_\nu^{(1s)} d\nu \int B_{12}(\nu - \nu') n_{\nu'} d\nu' = \frac{3c^3}{8\pi\nu_L^2} A_{21} \frac{n_{1s}}{\sqrt{\pi}(\Delta\nu)_D} \int n_\nu e^{-\frac{(\nu-\nu_0)^2}{(\Delta\nu)_D^2}} d\nu. \quad (7)$$

Of course, a similar calculation can be carried out for the stimulated emission term.

Because the nebula is optically thick in Lyman- α , n_ν must be considered carefully. Were escape from the nebula the primary removal mechanism, then a steady state would result in which photons are created near line center, diffuse in frequency through resonant scattering and are effectively removed far out in the wings. The decrease in both creation rate and diffusion rate with frequency offset results in a nearly flat distribution (n_ν) out to the approximate frequency at which photons freely escape, beyond which it drops sharply (Capriotti 1966). We write this

frequency offset as $w(\Delta\nu)_D$, where w is a dimensionless parameter expressing the offset in terms of the Doppler width. We shall therefore assume that $n_\nu = n_{Ly\alpha}/[2w(\Delta\nu)_D]$ for $|\nu - \nu_D| < w(\Delta\nu)_D$, and $n_\nu = 0$ for $|\nu - \nu_D| > w(\Delta\nu)_D$, where $n_{Ly\alpha}$ is the density of Lyman- α photons. The $2p$ rate equation then becomes

$$(1 - f)\alpha n_i n_e + C_{sp} n_{2s} n_i + \frac{3c^3}{16\pi\nu_L^2 (\Delta\nu)_D} \frac{A_{21}}{w} \text{erf}(w) n_{Ly\alpha} n_{1s} = A_{21} n_{2p}. \quad (8)$$

Spontaneous emission completely dominates the depopulation of the $2p$ state and thus the other two terms that appeared on the right hand side of equation (3) have been dropped. Stimulated emission is negligible in comparison with spontaneous emission for any reasonable value of $n_{Ly\alpha}$. Indeed, equality of spontaneous and stimulated emission would imply a radiation pressure (due to Lyman- α) many orders of magnitude in excess of the thermal gas pressure. Also, the $2p \rightarrow 2s$ collision rate is negligible for any reasonable value of n_i . [We include these collisions terms insofar as they populate the $2s$ state, however. See equation (1).]

As we shall see, it is quite plausible that Lyman- α photons are absorbed by dust before significant frequency diffusion occurs. In this case n_ν will simply reflect the thermal distribution of atoms. The resulting $2p$ rate equation is identical to that given above provided we replace $\text{erf}(w)/w$ with $2\sqrt{2/\pi}$.

At low densities, Lyman- α photons are created at the rate at which recombinations lead to $2p$ states, i.e. $(1 - f)\alpha n_i n_e$. At high densities ($n_i > 10^4 \text{ cm}^{-3}$) $2s$ states may be collisionally converted to $2p$ states leading to additional Lyman- α photons, and thus the Lyman- α creation rate could be as large as $\alpha n_i n_e$, the total recombination rate. We therefore define the Lyman- α lifetime as

$$t_{Ly\alpha} = \frac{n_{Ly\alpha}}{h \alpha n_i n_e}, \quad (9)$$

where $1 - f \leq h \leq 1$. Since $2p$ states decay to the ground state much faster than they could be collisionally converted to $2s$, all recombinations to $2p$ are regarded as producing a Lyman- α photon. Thus, h could never be smaller than $1 - f$.

We define

$$S = \frac{3c^3}{16\pi\nu_L^2 (\Delta\nu)_D} \frac{A_{21}}{(1 - f)} \frac{h}{w} \text{erf}(w) \chi n_H t_{Ly\alpha}, \quad (10)$$

where $\chi = n_{1s}/n_H$, and n_H is the total hydrogen density (atomic plus ionized). The rate equations [(1) and (8)] can then be solved for the $2s$ and $2p$ populations:

$$n_{2s} = \frac{\alpha n_i n_e [f A_{21} + (1 - f)(1 + S) C_{ps} n_i]}{A_{21} (A_{2\gamma} + C_{sp} n_i) - C_{sp} C_{ps} n_i^2} \quad (11)$$

$$n_{2p} = \frac{\alpha n_i n_e [(1 - f)(1 + S) A_{2\gamma} + (1 + S - fS) C_{sp} n_i]}{A_{21} (A_{2\gamma} + C_{sp} n_i) - C_{sp} C_{ps} n_i^2}. \quad (12)$$

The dimensionless parameter S gives the rate at which $2p$ states are produced by captured Lyman- α radiation in terms of the $2p$ creation rate from recombination (at low densities).

The ratio $n_{2p}/(3n_{2s})$ provides a determination of the relative importance of Lyman- α pumping of the $2p$ states and whether a fine structure line is expected to appear in absorption or (stimulated) emission. If $n_{2p}/(3n_{2s}) > 1$, then the 9.9 GHz, $2s_{1/2}$ - $2p_{3/2}$ line will appear in emission, and the 1.1 GHz, $2s_{1/2}$ - $2p_{1/2}$ line will appear in absorption. Of course, $n_{2p}/(3n_{2s}) < 1$ implies the opposite. (This assumes that the two $2p$ states are populated according to their relative statistical weights. To evaluate cases in which $n_{2p}/(3n_{2s})$ is of order unity, it would be necessary to separately account for the rates at which $2p_{1/2}$ and $2p_{3/2}$ states are created and destroyed, including the collisional rates coupling these states.) From equations (11) and (12) it follows that $n_{2p}/(3n_{2s}) > 1$ if $S > S_{crit}$ where,

$$S_{crit} = \frac{3f}{(1-f)} \frac{A_{21}}{A_{2\gamma}} = 1.14 \times 10^8. \quad (13)$$

(The numerical value of S_{crit} corresponds to $f = 1/3$.) Because the $2p$ states naturally decay about 10^8 times faster than the $2s$ states, population equality thus requires a pumping rate some 8 orders of magnitude faster than the approximate rate at which $2s$ and $2p$ states are formed through recombination.

3. The Lyman- α Density in HII Regions

Determination of the Lyman- α density in HII regions is a complicated transfer problem. It may be, however, that the dominant mechanism for removing Lyman- α photons is quite straightforward, i.e. absorption by dust (Spitzer 1978). Thus, we eschew the noncoherent radiative transfer problem and find the upper limits to $t_{Ly\alpha}$ and S set by absorption. Other competing removal processes would reduce the lifetime, and therefore density, of Lyman- α photons, resulting in a lower value for S .

Using a silicate-graphite model for dust in HII regions (Aannestad 1989), with a dust-to-gas ratio of 0.009, the extinction at Lyman- α can be shown to be $N_H/(5.4 \times 10^{20} \text{ cm}^{-2})$ mag, where N_H is the column density of hydrogen. The albedo for this mixture is about 0.4 at Lyman- α (Draine & Lee 1984). The lifetime of Lyman- α photons against absorption by dust can then be calculated as $t_{Ly\alpha} = (3.3 \times 10^{10} \text{ cm}^{-3} \text{ s})/n_H$. We then find that

$$S = 4.2 \times 10^7 \chi \frac{h}{(1-f)} \frac{\text{erf}(w)}{w}. \quad (14)$$

Since $\chi \ll 1$ throughout most of the volume of an HII region (Osterbrock 1989), we conclude that $S \ll S_{crit}$ and that the $2s$ state is overpopulated relative to the $2p$ states.

In the harsh environments of planetary nebulae dust might be destroyed by shocks or hard UV radiation, or possibly separated from the ionized gas by radiation pressure (Natta & Panagia 1981; Pottasch 1987). Abundance measurements indicate, however, that various heavy elements are depleted from the gas phase in the ionized regions of NGC 7027 (Kingdon & Ferland 1997) and NGC 6445 (van Hoof et al. 2000), suggesting that dust has not been destroyed in significant quantities. Additionally, planetary nebulae frequently exhibit a mid-IR spectral component characteristic of

warm dust heated by the intense radiation field within the ionized region (Kwok 1980; Hoare 1990; Hoare et al. 1992). Summarizing these results, Barlow (1993) has argued that dust is a common constituent of the ionized zones of planetary nebulae, albeit with dust-to-gas ratios about an order of magnitude or more below that of the general ISM.

Middlemass (1990) has modeled NGC7027 and finds an extinction optical depth of about 0.17 at 500.7 nm. For a uniform model the column density of hydrogen in the ionized zone is about $3.5 \times 10^{21} \text{ cm}^{-2}$ (Thomasson & Davies 1970), along the radius of the nebula. For the graphite dust model used by Middlemass (1990) the extinction at Lyman- α then is $N_H/(1.3 \times 10^{22} \text{ cm}^{-2})$ mag; about a factor of 20 smaller than that in a general HII region described above, and roughly consistent with the smaller dust-to-gas ratio ($\approx 7 \times 10^{-4}$) in this object (Barlow 1993). For an albedo of 0.4, the Lyman- α lifetime is $t_{Ly\alpha} = (7.6 \times 10^{11} \text{ cm}^{-3} \text{ s})/n_H$, and thus

$$S \approx 9.8 \times 10^8 \chi \frac{h}{(1-f)} \frac{\text{erf}(w)}{w}. \quad (15)$$

If we assume that absorption by dust is the dominant process limiting the Lyman- α density, and make the replacement $\text{erf}(w)/w \rightarrow 2\sqrt{2/\pi}$, and let $h \approx 1$, we obtain $S = 2.3 \times 10^9 \chi$. Since it is quite unlikely that χ is as large as 0.05, as required for $S \approx S_{crit}$, we conclude also in this case that the $2p$ states are underpopulated relative to the $2s$ states.

Of course, the above estimates are upper limits to the Lyman- α lifetime, as other processes (described in Section 1) may contribute to the removal of these photons. Thus, values of S estimated in this way are upper limits. In addition, if escape is important then the relevant value of $\text{erf}(w)/w$ would be smaller than that substituted above.

It should also be noted that Lyman- α radiation contributes to heating the dust in the ionized region. The energy absorbed is then reradiated in the IR. In the case of NGC 7027 a mid-IR spectral component is evidently due to dust with temperature $T_d \approx 230$ K comixed with the ionized gas (Kwok 1980). If the heating is dominated by Lyman- α radiation, then

$$n_{Ly\alpha} h \nu_L c Q_{abs}(Ly\alpha) = 4 \langle Q(a, T_d) \rangle \sigma T_d^4, \quad (16)$$

where $Q_{abs}(Ly\alpha)$ is the absorption efficiency at Lyman- α and $\langle Q(a, T_d) \rangle$ is the Planck-averaged emissivity (Draine & Lee 1984), a function of grain size a and temperature T . Large grains, being efficient emitters in the IR, will yield a larger estimate of $n_{Ly\alpha}$. Thus, we assume 1 μm graphite grains for which $Q_{abs}(Ly\alpha) \approx 1$ and $\langle Q(1 \mu\text{m}, 230 \text{ K}) \rangle \approx 0.05$ (Draine & Lee 1984). Then,

$$n_{Ly\alpha} = \frac{4\sigma T^4 \langle Q(1 \mu\text{m}, 230 \text{ K}) \rangle}{h \nu_L c Q_{abs}} = 6.5 \times 10^4 \text{ cm}^{-3}. \quad (17)$$

We then find

$$S = \frac{3c^3}{16\pi\nu_L^2} \frac{A_{21}}{(\Delta\nu)_D} \frac{1}{\alpha(1-f)} \frac{\text{erf}(w)}{w} \frac{\chi}{(1-\chi)} \frac{n_{Ly\alpha}}{n_e} = 2.6 \times 10^{10} \frac{\text{erf}(w)}{w} \frac{\chi}{(1-\chi)}, \quad (18)$$

where we have taken $n_i = (1 - \chi)n_H$ (since the fraction of atoms in excited, bound states is negligible). To obtain the numerical value given above we used the recombination coefficient in the density bounded case with $T = 10^4$ K (Osterbrock 1989). Assuming Lyman- α radiation is primarily removed through absorption by dust (in which case $\text{erf}(w)/w$ is replaced by $2\sqrt{2/\pi}$), then $S < S_{\text{crit}}$ unless χ exceeds 2.4×10^{-3} , which is unlikely (Osterbrock 1989). It should also be noted that other sources, such as continuum radiation, are likely important in heating the dust, thereby reducing further the implied value of $n_{Ly\alpha}$ (and therefore S). Finally, the $1 \mu\text{m}$ grain size assumed here is probably an overestimate implying that $n_{Ly\alpha}$ is also overestimated.

4. Radiative Transfer of the Fine Structure Lines

Evidently, the $2s$ state is overpopulated relative to $2p$, thus the fine structure transitions will proceed from $2s_{1/2}$ to $2p_{3/2}$ via absorption and to $2p_{1/2}$ via stimulated emission. Although the $2p$ populations are probably negligible, they will be included in the radiative transfer calculation. The distribution of $2p$ states between $2p_{1/2}$ and $2p_{3/2}$ may deviate somewhat from the statistical weights (1/3 and 2/3, respectively), in part because the separate collisional rates from $2s$ are not proportional to the statistical weights. Since the $2p$ population is most likely negligible, a detailed calculation of the distribution between $2p_{1/2}$ and $2p_{3/2}$ states will not be carried out here. Rather, the fractional populations of $2p_{1/2}$ and $2p_{3/2}$ will be parameterized as $\beta_a/3$ and $2\beta_b/3$, respectively. If $\beta_a = \beta_b = 1$, then these states are populated according to their statistical weights. There is the obvious constraint that $\beta_a/3 + 2\beta_b/3 = 1$.

The fine structure transitions are allowed electric dipole transitions and the corresponding rates may be computed in a straightforward manner (Bethe & Salpeter 1957), giving $A_a = 1.597 \times 10^{-9} \text{ sec}^{-1}$ ($2s_{1/2}$ – $2p_{1/2}$) and $A_b = 8.78 \times 10^{-7} \text{ sec}^{-1}$ ($2p_{3/2}$ – $2s_{1/2}$). The absorption coefficient (valid for either transition) is

$$\kappa_\nu = \pm \frac{c^2}{8\pi\nu^2} \frac{g}{g_{2s}} A_\nu (n_{2s} - \frac{\beta}{3} n_{2p}), \quad (19)$$

where g is the degeneracy of the final state (2 for $2p_{1/2}$, 4 for $2p_{3/2}$; $g_{2s} = 2$). The $-$ sign corresponds to transitions to $2p_{1/2}$; the $+$ sign to transitions to $2p_{3/2}$, and β is either β_a or β_b , respectively. Either final state quickly decays to the ground state via Lyman- α with rate A_{21} . The natural line width of the $2s$ – $2p$ transitions is therefore dominated by the rapid decay of the $2p$ state and is $\Gamma = A_{21}/2\pi = 99.8 \text{ MHz}$. For a Lorentzian profile,

$$A_\nu = \frac{A(\Gamma/2\pi)}{(\nu - \nu_f)^2 + (\Gamma/2)^2}, \quad (20)$$

where A is either A_a or A_b and ν_f is the frequency of the fine structure transition. From equations (11) and (12) we find

$$n_{2s} - \frac{\beta}{3} n_{2p} = \frac{f\alpha n_i n_e}{(A_{2\gamma} + C_{sp} n_i)} \left(1 - \frac{\beta S}{S_{\text{crit}}}\right), \quad (21)$$

where we have assumed that the Lyman decay rate A_{21} always dominates the collision rate $C_{sp}n_i$. The absorption coefficient at line center then is

$$\kappa_{\nu}^{max} = \pm \frac{c^2}{8\pi\nu_f^2 g_{2s}} \frac{g}{\pi\Gamma} \frac{2A}{(A_{2\gamma} + C_{sp}n_i)} \frac{f\alpha n_i n_e}{(1 - \frac{\beta S}{S_{crit}})}. \quad (22)$$

This will be scaled according to the free-free absorption coefficient (Altenhoff et al. 1960),

$$\kappa_{\nu}^{ff} \approx \frac{0.212 n_i n_e}{v^{2.1} T^{1.35}}. \quad (23)$$

The ratio of the line optical depth (at line center), τ_{ν}^{max} , to the free-free continuum optical depth, τ_{ν}^{ff} , then is

$$R = \frac{\tau_{\nu}^{max}}{\tau_{\nu}^{ff}} = \frac{K}{(A_{2\gamma} + C_{sp}n_i)} \left(1 - \frac{\beta S}{S_{crit}}\right), \quad (24)$$

where $K = -3.0 \times 10^{-4}$ sec $^{-1}$ for the $2s_{1/2} \rightarrow 2p_{1/2}$ transition and $K = 0.41$ sec $^{-1}$ for the $2s_{1/2} \rightarrow 2p_{3/2}$ transition. We assumed $T = 10^4$ K, and that all ionizing photons are captured by the HII region (Osterbrock 1989).

The equation of transfer is

$$\frac{dI_{\nu}}{dx} = (-\kappa_{\nu}^{ff} - \kappa_{\nu})I_{\nu} + J_{\nu}^{ff}. \quad (25)$$

Note that the line produces absorption or stimulated emission only (through κ_{ν}), but does not produce significant spontaneous emission. Thus, the emissivity is completely dominated by the free-free emissivity, J_{ν}^{ff} . For an HII region uniform along a ray path the solution is

$$T_b = T \frac{1 - e^{-(1+R)\tau_{\nu}^{ff}}}{1 + R}, \quad (26)$$

where the result has been expressed in terms of brightness temperature T_b . The line strength (in K) divided by the continuum brightness temperature is

$$\frac{\Delta T_b}{T_{b,cont}} = \frac{1}{1 + R} \frac{e^{\tau_{\nu}^{ff}} - e^{-R\tau_{\nu}^{ff}}}{e^{\tau_{\nu}^{ff}} - 1} - 1. \quad (27)$$

In the optically thin limit ($\tau_{\nu}^{ff} \ll 1$) expanding (to second order) gives

$$\frac{\Delta T_b}{T_{b,cont}} = -\frac{1}{2} R \tau_{\nu}^{ff} = -\frac{1}{2} \tau_{\nu}^{max}. \quad (28)$$

In the optically thick limit ($\tau_{\nu}^{ff} \gg 1$),

$$\frac{\Delta T_b}{T_{b,cont}} = \frac{-R}{1 + R}. \quad (29)$$

The lines do not disappear in the optically thick limit as long as the $2s$ and $2p$ states are not in equilibrium. The 10^4 K microwave radiation field is not sufficient to overcome the rates described

in Section 2 and thus it can not establish equilibrium. For example, in the likely case where $n_{2p}/(3n_{2s}) \ll 1$, the $2p$ levels are drained by Lyman- α emission faster than the microwave radiation field can return these states to $2s$ via either absorption or stimulated emission. (See also Section 2.)

Each fine structure level is split into two hyperfine levels as shown in Figure 1. The allowed transitions are also indicated. Both fine structure lines are split into three hyperfine components. The relative intensities of the components can be calculated from the appropriate sum rules (Sobelman 1992). For the 910, 1088, and 1147 MHz lines the ratios are 1:2:1. The 9852, 9876, and 10030 MHz lines appear in the ratios 1:5:2.

5. Prospects for Detection

The 9.9 GHz transitions are intrinsically about three orders of magnitude stronger than the 1.1 GHz transitions. The solution to the radiative transfer equation indicates that, in general, the line brightness temperature ΔT_b grows as the square of the free-free optical depth in the optically thin limit (equation 28). One factor comes from the growth of free-free emission, which effectively forms the “background”, and the other from the proportionate growth of the line absorption. In the optically thick limit, the growth in line temperature saturates (equation 29). Most HII regions of interest are optically thin at 9.9 GHz and optically thick at 1.1 GHz. In general, the higher optical depth at 1.1 GHz does not significantly offset the relative weakness of these transitions. We find, therefore, that the 9.9 GHz lines offer the better prospects for detection.

Table 1 gives estimates of the line strengths for various HII regions and components, and planetary nebulae. It was assumed that $S = 0$, in which case the 9.9 GHz lines would appear in absorption and the 1.1 GHz lines in stimulated emission. Most of the entries in Table 1 correspond to high emission measure components in HII regions, which are listed according to the nomenclature of the original references. The published emission measure values E were used to calculate the free-free optical depth and the continuum brightness temperature (assuming in most cases $T_e \approx 10^4$ K). The line-to-continuum optical depth ratios R are calculated from the published electron densities (equation 24).

The estimates in Table 1 take into account the distribution of the line strength over three hyperfine components making up each fine structure line and the consequent line blending. At 9.9 GHz, the strongest line (9876 MHz) will be blended with the weakest line (9853 MHz). The peak temperature occurs at 9874 MHz and is 75% of that calculated using equation 26 for a single (fictitious) fine structure line. The 10030 MHz line will be somewhat distinct with a peak temperature equal to 32% of that predicted from equation 26, including contributions from the wings of the 9852 and 9876 MHz lines. The situation at 1.1 GHz is similar. The 1088 MHz line will appear blended with the 1147 MHz line, with a peak value of 63% at 1093 MHz. The 910 MHz line will remain distinct with a peak value of 30%, including line wing contributions from the

other two lines. The estimates in Table 1 give the line temperature at the peak of the brightest spectral feature in either the 9.9 GHz or 1.1 GHz blended multiplet. At both frequencies, the resulting profile of a strong blended feature and a distinct weaker line, combined with Lorentzian line shapes, will provide a unique detection signature. Figure 2 shows the predicted appearance of the blended multiplet around 9.9 GHz.

The Green Bank Telescope (GBT) provides a realistic hope of detection of the 9.9 GHz lines. Having a clear aperture it should be relatively free of standing waves in the antenna structure. Thus, it should be possible to search for very broad spectral features over bandpasses as large as 800 MHz. Nevertheless, the high emission measure HII regions that are likely to show the lines are typically quite compact. Therefore, the estimated line antenna temperatures (ΔT_a)_{9.9} include the effects of dilution in the 1'.21 GBT beam. The estimated values of ΔT_a at 1.1 GHz were calculated using either the 11' GBT beam (subscript *G*), or where appropriate, the Arecibo 4'.3 beam (subscript *A*).

Quite possibly the observational sensitivity will be limited by systematic effects in which the continuum antenna temperature is modulated by frequency dependent gain variations which are not entirely removed by calibration procedures. Thus the limiting factor may be the line-to-continuum ratio, $\Delta T/T$, which is also tabulated for both lines.

The estimates given in Table 1 are only approximate. The underlying observations are biased in favor of component sizes to which various interferometer arrays are sensitive. In complex HII regions structures are present on a range of scales, down to very high emission measure arc-second scale components (Turner & Matthews 1984). The components included in the table (typically a few tens of arc seconds in size) were selected because they contribute significantly to the total flux in the GBT beam. The more compact, arc-second scale components typically yield larger values of $\Delta T/T$ (despite densities $> 10^4 \text{ cm}^{-3}$ and consequent collisional de-excitation), yet they tend to contribute relatively little to the total flux in the GBT beam. Conversely, extended, low emission measure components in the beam will add to the antenna temperature while contributing little line absorption. It should also be noted that the presence of structures having a wide range of densities implies that the uniform model considered in Section 4 is an oversimplification. Inhomogeneous structure, including clumping, in the emission regions would imply that the emission measure estimates in Table 1 represent an average over the surface of the source. In the optically thin case, i.e. most sources at 9.9 GHz, a redistribution of emission measure, and therefore optical depth, will tend to strengthen the overall estimated line strength ΔT_b due to its τ^2 -dependence (equation 28). Collisional de-excitation in denser regions of the source, however, will tend to reduce the line optical depth (equation 24). Because R is density dependent, particularly for densities above about $1.5 \times 10^4 \text{ cm}^{-3}$, the brightness temperature for a homogeneous source (equation 26) cannot be rescaled using some weighted optical depth; rather, detailed modeling would be required.

Three high emission measure planetary nebulae are also included in the table (IC 418, NGC 7027, and NGC 6572). These objects tend to have somewhat simpler structure than the more

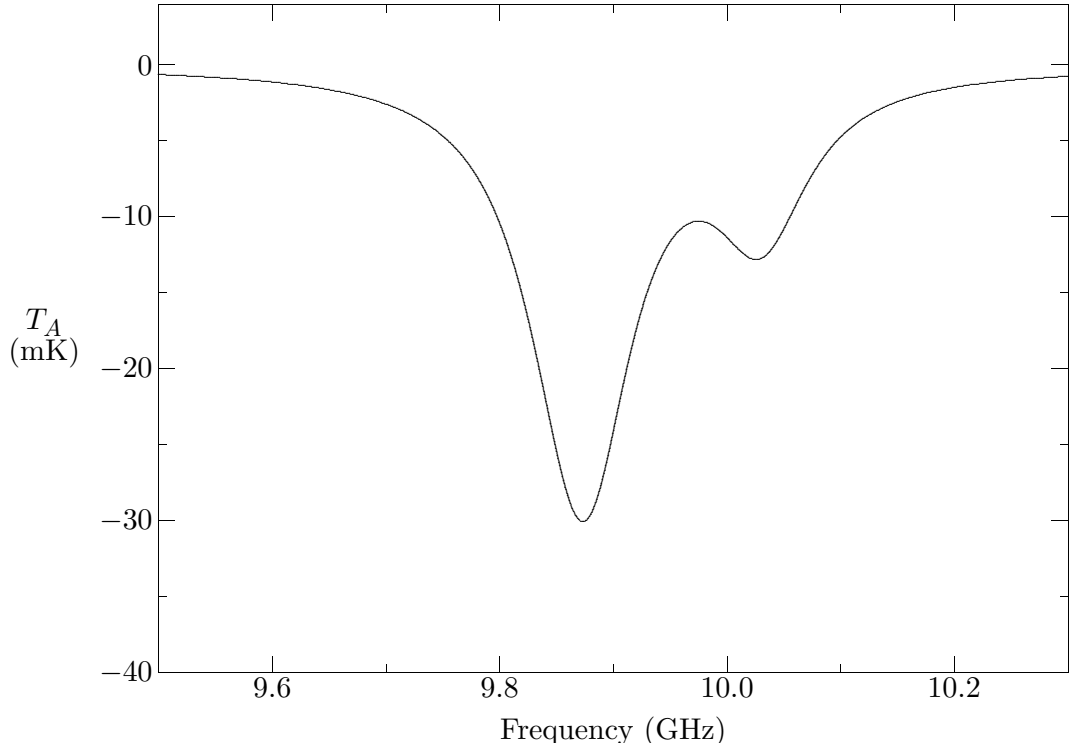


Fig. 2.— Hyperfine multiplet near 9.9 GHz. Three hyperfine components at 9.852, 9.876, and 10.030 GHz appear blended due to the large natural line width, 99.8 MHz, of these transitions. The individual line strengths are in the ratio 1:5:2. The vertical axis is the predicted antenna temperature for Green Bank Telescope observations of NGC 7027, corresponding to the shell model, listed in Table 1 as $\{\text{NGC 7027}\}_S$. The relative populations of the $2p$ states are assumed negligible (see text), and thus the 9.9 GHz lines appear in absorption. The line profiles are completely dominated by natural line width and thus strong Lorentzian wings are apparent.

complex HII regions. Nevertheless, NGC 7027 has a well documented shell structure. In this case, a number of emission line diagnostics indicate $n_e \approx 5 \times 10^4 \text{ cm}^{-3}$ (Middlemass 1990). Subarcsecond radio images show that the emission originates from a shell with a peak emission measure of about $2.7 \times 10^8 \text{ pc cm}^{-6}$ (Bryce et al. 1997). Both results are consistent with an area filling factor of about 30%, with characteristic emission measure of about $1.2 \times 10^8 \text{ pc cm}^{-6}$. The higher emission measure boosts the line-to-continuum ratio, whereas the higher density acts oppositely due to collisional de-excitation. The net result in this case is a somewhat stronger estimated line with $\Delta T_b/T_{b,cont} \approx -1.4 \times 10^{-3}$. This case is worked out in Table 1 as $\{\text{NGC 7027}\}_S$, and depicted in Figure 2.

Generally, compact, high emission measure objects tend to give stronger line-to-continuum ratios, despite their higher densities (which result in collisional de-excitation). This is because HII regions tend to be loosely organized along domains of constant excitation parameter U (Habing & Israel 1979). Using size d as a free parameter, then $E \propto U^3/d^2$. For $E < 3.8 \times 10^8 \text{ pc cm}^{-6}$, the HII region is optically thin at 9.9 GHz and, for $S = 0$

$$\frac{\Delta T_b}{T_{b,cont}} \approx -10^{-2} \frac{E_8}{n_4 + 1.5} \quad (30)$$

where $E_8 = E/(10^8 \text{ pc cm}^{-6})$ and $n_4 = n/(10^4 \text{ cm}^{-3})$. Thus, in the low density limit ($n_4 \ll 1.5$) the line-to-continuum ratio grows in direct proportion to E , and therefore to d^{-2} for fixed U . Of course, the most compact objects have densities in excess of $1.5 \times 10^4 \text{ cm}^{-3}$, in which case the line-to-continuum ratio increases with $d^{-1/2} \propto E^{1/4}$ for fixed U , since $n_e \propto (U/d)^{3/2}$. For emission measures above $\approx 4 \times 10^8 \text{ pc cm}^{-6}$ an HII region becomes optically thick at 9.9 GHz and the advantage of increased emission measure is lost. In such cases, higher densities will reduce the line-to-continuum ratio.

As discussed above, the 1.1 GHz lines are considerably weaker. Under the most favorable conditions of high free-free optical depth and low density, we find

$$\frac{\Delta T_b}{T_{b,cont}} \approx -R \approx 3.6 \times 10^{-5}, \quad (31)$$

assuming, as discussed above, that $S = 0$. These conditions are not uncommon and exceptionally high emission measures are not required to achieve high optical depth at 1.1 GHz. In the case of M 42 the optical depth at 1.1 GHz is 1.2 and the beam diluted line strength would be about 4 mK, versus a continuum antenna temperature of $\approx 400 \text{ K}$.

6. Conclusions

The metastable $2s_{1/2}$ state of hydrogen is likely overpopulated in HII regions. Lyman- α pumping of the $2p$ states is expected to be negligible due to absorption of Lyman- α radiation by dust. Thus the $2s_{1/2} \rightarrow 2p_{3/2}$ transitions (9.9 GHz) are predicted to appear in absorption and the

$2s_{1/2} \rightarrow 2p_{1/2}$ transitions (1.1 GHz) in stimulated emission. Because of the short lifetime of the final $2p$ states, the width of the lines is dominated completely by intrinsic line width. In effect, then, the power is distributed over ≈ 100 MHz of line width resulting in very weak lines. In addition, the power is distributed over three strongly blended hyperfine lines in each multiplet.

Searching for the 9.9 GHz lines in high emission measure HII regions offers the best prospects for detection. In the optically thin limit, the line strength varies as the square of the free-free optical depth. Predicted line-to-continuum ratios (in absorption) range up to several tenths of a percent in W58A, including the effects of line blending. With the Green Bank Telescope, the predicted peak absorption line strength may reach $\Delta T_a \approx -170$ mK in this case, allowing for the redistribution of line strength over the three hyperfine lines. Other high emission HII regions are expected to show somewhat weaker 9.9 GHz lines, for example with line-to-continuum ratios of about 0.1 percent and line strengths of tens of mK with the Green Bank Telescope. These predictions are uncertain, however, owing to biases inherent in estimating emission measures as well as selection effects in various interferometric surveys of compact HII regions.

These conclusions apply to thermal sources. An important extension of this work would consider the broad line regions of active galactic nuclei and quasars in which a strong nonthermal microwave radiation field could influence the populations of the $2s$ and $2p$ levels, as well as provide a background for line absorption or stimulated emission.

In general, detection of the fine structure lines of hydrogen will be challenging due to the extraordinary line width and blended structure. The observation will require meticulous baseline calibration and subtraction.

We thank Drs. R. Brown and J. Simonetti for useful discussions. Portions of this work were completed while one of the authors (B.D.) was a Visiting Scientist at the National Radio Astronomy Observatory (NRAO) in Green Bank, WV, and also a faculty member in the Department of Physics at Virginia Tech. This work was supported by the Glaxo-Wellcome Endowment at the University of North Carolina-Asheville and by National Science Foundation grant AST-0098487 to Virginia Tech. The National Radio Astronomy Observatory is a facility of the National Science Foundation operated under cooperative agreement by Associated Universities, Inc.

REFERENCES

Aannestad, P. A. 1989, *ApJ*, 338, 162

Altenhoff, W., Mezger, P. G., Wendker, H., & Westerhout, G. 1960, *Veröff Univ. Sternwarte, Bonn*, 59, 48

Barlow, M. J. 1993, in *Planetary Nebulae, Proceedings of the 155 Symposium of the IAU*, eds. R. Weinberger & A. Acker (Dordrecht: Kluwer), 163

Bethe, H. A. & Salpeter, E. E. 1957, Handbuch der Physik, Band 35, Atome 1, 1

Breit, G. & Teller, E. 1940, ApJ, 91, 215

Bryce, M., Pedlar, A., Muxlow, T., Thomasson, P., & Mellema, G. 1997, MNRAS, 284, 815

Capriotti, E. R. 1966, ApJ, 146, 709

Cox, D. P. & Matthews, W. G. 1969, ApJ, 155, 859

Draine, B. T. & Lee H. M. 1984, ApJ, 285, 89

Field, G. B. & Partridge, R. B. 1961, ApJ, 134, 959

Habing, H. J. & Isreal, F. P. 1979, ARA&A, 17, 345

Hoare, M. G. 1990, MNRAS, 244, 193

Hoare, M. G., Roche, P. F., & Clegg, R. E. S. 1992, MNRAS, 258, 257

Kingdon, J. B. & Ferland, G. J. 1997, ApJ, 477, 732

Krassner, J., Pipher, J. L., Savedoff, M. P., & Soifer, B. T. 1983, AJ, 88, 972

Kwok, S. 1980, ApJ, 236, 592

Middlemass, D. 1990, MNRAS, 244, 294

Myers, P. C. & Barrett, A. H. 1972, ApJ, 176, 111

Natta, A. & Panagia, N. 1981, ApJ, 248, 189

Osterbrock, D. E. 1989, *Astrophysics of Gaseous Nebulae and Active Galactic Nuclei* (Mill Valley: University Science Books)

Pottasch, S. R. 1960, ApJ, 131, 202

Pottasch, S. R. 1986, in *Late Stages of Stellar Evolution*, eds. S. Kwok & S. R. Pottasch, (Dordrecht: D. Reidel)

Purcell, E. M. 1952, ApJ, 116, 457

Seaton, M. J. 1955, Proc Roy Soc London A, 68, 457

Schraml, J. & Mezger, P. G. 1969, ApJ, 156, 269

Shklovski, I. S. 1960, *Cosmic Radio waves* (Cambridge: Harvard University Press), 255

Sobelman, I. I. 1992, *Atomic Spectra and Radiative Transitions* (Berlin: Springer)

Spitzer, L. 1978, Physical Processes in the Interstellar Medium (New York: Wiley-Interscience)

Spitzer, L. & Greenstein, J. L. 1951, *ApJ*, 114, 407

Thomasson, P & Davies, J. G. 1970, *MNRAS*, 150, 359

Townes, C. H. 1957, in Radio Astronomy, Proceeding from 4th IAU Symposium, ed. H. C. Van de Hulst (Cambridge: Cambridge Univ. Press), 92

Turner, B. E. & Matthews, H. E. 1984, *ApJ*, 277, 164

van Gorkom, J. H., Goss, W. M., Shaver, P. A., Schwartz, U. J., & Harten, R. H. 1980, \AA , 89, 150

van Hoof, P. A. M., Van de Steene, G. C., Beintema, D. A., Martin, P. G., Pottasch, S. R., & Ferland, G. J. 2000, *ApJ*, 532, 384

Webster, W. J. & Altenhoff, W. J. 1970, *AJ*, 75, 896

Wild, J. P., *ApJ*, 115, 206

Wynn-Williams, C. G. 1971, *MNRAS*, 151, 397

Table 1. HII Regions — Estimated line strengths.

HII Region	n_e (cm $^{-3}$)	E (pc cm $^{-6}$)	θ	$\tau_{9.9}^{ff}$	$R_{9.9}$	$\left(\frac{\Delta T_b}{T_{b,cont}}\right)_{9.9}$	$\left(\Delta T_a\right)_{9.9}$ (mK)	$R_{1.1}$	$\left(\frac{\Delta T_b}{T_{b,cont}}\right)_{1.1}$	$\left(\Delta T_a\right)_{1.1}$ (mK)	Reference
W3.1	8200	1.6×10^7	$12'' \times 10''$	0.043	0.033	-5.2×10^{-4}	-5.0	-2.4×10^{-5}	1.4×10^{-5}	0.04_G	1
W3.4	5700	1.2×10^7	$20'' \times 15''$	0.032	0.036	-4.2×10^{-4}	-7.5	-2.7×10^{-5}	1.4×10^{-5}	0.10_G	1
W3.5	6100	1.4×10^7	$20'' \times 15''$	0.037	0.035	-5.0×10^{-4}	-10.	-2.6×10^{-5}	1.5×10^{-5}	0.10_G	1
IC 418	2.6×10^4	7.7×10^6	$11.''5$	0.020	0.019	-1.4×10^{-4}	-0.7	-1.4×10^{-5}	6.0×10^{-6}	0.02_G	2
M42	2200	3.2×10^6	$2.''6 \times 3.''5$	0.012	0.044	-1.9×10^{-4}	-17.	-3.2×10^{-5}	9.4×10^{-6}	3.7_G	3
NGC6572	2.5×10^4	3.2×10^7	$6.''4$	0.085	0.019	-6.1×10^{-4}	-4.0	-1.4×10^{-5}	8.8×10^{-6}	0.053_G	2
M17	950	2.4×10^6	$4.''5 \times 1.''8$	0.064	0.047	-1.1×10^{-4}	-7.5	-3.4×10^{-5}	6.3×10^{-6}	2.1_G	3
W48	8075	1.8×10^7	$11'' \times 28''$	0.048	0.033	-5.8×10^{-4}	-16.	-2.4×10^{-5}	1.5×10^{-5}	0.63_A	4
W49A.1	5000	1.6×10^7	$7.''$	0.043	0.038	-5.8×10^{-4}	-2.5	-2.8×10^{-5}	1.6×10^{-5}	0.13_A	5
W49A.4	7000	3.1×10^7	$7.''$	0.083	0.034	-1.0×10^{-3}	-8.2	-2.5×10^{-5}	1.6×10^{-5}	0.13_A	5
W49A.5	4000	1.9×10^7	$15''$	0.051	0.040	-7.4×10^{-4}	-16.	-2.9×10^{-5}	1.8×10^{-5}	0.59_A	5
W49A.6	4000	1.4×10^7	$11''$	0.037	0.040	-5.5×10^{-4}	-4.6	-2.9×10^{-5}	1.6×10^{-5}	0.28_A	5
W51A.b	4800	1.1×10^7	$12''$	0.029	0.038	-4.1×10^{-4}	-3.3	-2.8×10^{-5}	1.4×10^{-5}	0.30_A	5
W51A.d	1.2×10^4	4.4×10^7	$7''$	0.012	0.028	-1.2×10^{-3}	-13.	-2.1×10^{-5}	1.3×10^{-5}	0.10_A	5
W51A.e	5000	2.1×10^7	$21''$	0.056	0.038	-7.5×10^{-4}	-37.	-2.8×10^{-5}	1.7×10^{-5}	1.1_A	5
W58A	3.9×10^4	3.5×10^8	$6''$	0.931	0.014	-4.2×10^{-3}	-170.	-1.0×10^{-5}	6.3×10^{-6}	0.04_A	6
DR 21	1.2×10^4	3.4×10^7	$20'' \times 7''$	0.091	0.028	-1.0×10^{-3}	-23.	-2.1×10^{-5}	1.3×10^{-5}	0.04_G	6
NGC 7027	1.9×10^4	4.2×10^7	$11.''5$	0.11	0.023	-1.0×10^{-3}	-25.	-1.7×10^{-5}	1.0×10^{-5}	0.03_G	2
{NGC 7027} $_S^a$	5.0×10^4	1.3×10^8	$\sqrt{3}11.''5$	0.34	0.012	-1.4×10^{-3}	-30.	-8.6×10^{-5}	5.4×10^{-5}	0.05_G	7

^aShell model for NGC 7027. See text.

Note. — Antenna temperatures (ΔT_a) include the effects of beam dilution with the Green Bank Telescope at 9.9 GHz and 1.1 GHz (indicated by subscript G), and Arecibo at 1.1 GHz (subscript A).

References. — (1) Webster & Altenhoff 1970; (2) Thomasson & Davies 1970; (3) Schraml & Mezger 1969; (4) Krassner et al. (1983); (5) van Gorkom et al. (1980); (6) Wynn-Williams (1971); (7) Bryce et al. 1997